

Faraday rotation and circular dichroism spectra of gold and silver nanoparticle aggregates

Sahar Pakdel and MirFaez Miri*

Department of Physics, University of Tehran, P. O. Box 14395-547, Tehran, Iran

(Received 6 October 2012; revised manuscript received 22 November 2012; published 26 December 2012)

We study the magneto-optical response of noble metal nanoparticle clusters. We consider the interaction between the light-induced dipoles of particles. In the presence of a magnetic field, the simplest achiral cluster, a dimer, exhibits circular dichroism (CD). The CD of a dimer depends on the directions of the magnetic field and the light wave vector. The CD of a populous cluster weakly depends on the magnetic field. Upon scattering from the cluster, an incident linearly polarized light with polarization azimuth φ becomes elliptically polarized. The polarization azimuth rotation and ellipticity angle variation are sinusoidal functions of 2φ . The anisotropy and the chirality of the cluster control the amplitude and offset of these sinusoidal functions. The Faraday rotation and Faraday ellipticity are also sinusoidal functions of 2φ . Near the surface plasmon frequency, Faraday rotation and Faraday ellipticity increase.

DOI: [10.1103/PhysRevB.86.235445](https://doi.org/10.1103/PhysRevB.86.235445)

PACS number(s): 78.20.Ls, 78.67.Bf, 73.20.Mf, 78.20.Fm

I. INTRODUCTION

The magneto-optical (MO) response of nanocomposites has attracted a lot of interest. In view of potential applications in information storage, magnetic field sensors, switches, modulators, optical isolators, circulators, and deflectors,^{1,2} composites containing γ -Fe₂O₃, CoFe₂O₄, Fe₃O₄, Co, and Fe nanoparticles are studied.^{3–9} Recent advances in plasmonics have led to the introduction of *magnetoplasmonic* nanostructures composed of ferromagnets and noble metals. The large MO response of magnetoplasmonic composites can be understood heuristically: The metallic constituent sustains localized or propagating surface plasmons. This gives rise to enhanced electromagnetic field intensity inside the ferromagnetic constituent which exhibits the MO activity. Magnetoplasmonic crystals,¹⁰ metal films with arrays of holes filled with a magneto-optically active material,^{11,12} subwavelength-perforated conducting films in the presence of a magnetic field,^{13,14} periodic metal-dielectric composite films,¹⁵ Fe/Cu bilayer films,¹⁶ Ag/Co/Ag and Au/Fe/Au systems,^{17,18} Au-coated γ -Fe₂O₃ nanoparticles,^{19,20} and dumbbell-like Ag-CoFe₂O₄ nanoparticle pairs^{21,22} are thoroughly studied.

Recently, Sepúlveda *et al.*²³ have experimentally demonstrated that pure noble metal nanoparticles exhibit measurable MO response at low magnetic fields (about 10^4 G). This effect was attributed to the Lorentz force induced by the collective motion of the conduction electrons in the nanoparticle when the localized surface plasmon resonance is excited. In this experiment, the particles were not in close proximity, and thus the interparticle coupling effect²⁴ was weak.

In this paper, we study the interparticle coupling effect on the MO activity of gold and silver nanoparticle aggregates. We rely on the celebrated dipole approximation. In this approximation, a particle with diameter much less than the light wavelength is represented as a dipole. The local electric field acting on any dipole is a superposition of the incident light field and secondary fields produced by other dipoles. We assume that the aggregate interacts with the external static magnetic field \mathbf{B} and linearly polarized light specified by the polarization azimuth φ . Using the azimuth φ_s and ellipticity angle μ to characterize the vibration ellipse of the field scattered by the aggregate, we find that the polarization

azimuth rotation $\Delta = \varphi_s - \varphi$ and ellipticity angle variation μ can be expressed as

$$\begin{aligned}\Delta(\varphi) &= \Delta_{\text{str}}(\varphi) + B\Delta_{\text{Far}}(\varphi), \\ \mu(\varphi) &= \mu_{\text{str}}(\varphi) + B\mu_{\text{Far}}(\varphi).\end{aligned}\quad (1)$$

The term Δ_{str} (μ_{str}), which does not depend on the magnetic field, describes the structural polarization azimuth rotation (structural ellipticity angle variation), a manifestation of the *anisotropy* and *chirality* of the aggregate. The term $B\Delta_{\text{Far}}$ ($B\mu_{\text{Far}}$), which is proportional to the magnetic field, describes the Faraday rotation (Faraday ellipticity). We find that near the plasmon resonance of the noble metal, both Δ_{Far} and μ_{Far} increase. We find that

$$\begin{aligned}\Delta_{\text{str}}(\varphi) &\approx \Delta_1 \sin(2\varphi - 2\varphi_0) + \Delta_2, \\ \mu_{\text{str}}(\varphi) &\approx \mu_1 \sin(2\varphi - 2\varphi'_0) + \mu_2,\end{aligned}\quad (2)$$

where Δ_i and μ_i depend on the light frequency, host medium dielectric constant, nanoparticle radius, etc., and Δ_{Far} and μ_{Far} are also a sinusoidal function of 2φ . For the simplest anisotropic and achiral cluster, a dimer, we find that $\Delta_2 = 0$ and $\mu_2 = 0$. For a set of nanoparticles positioned on a helix, $\Delta_2 \neq 0$ and $\mu_2 \neq 0$. For a random gas of particles, which is anisotropic and chiral to some extent, $\Delta_2 \neq 0$ and $\mu_2 \neq 0$. The significance of these results may be seen better by considering the optical response of a bulk medium. For a *bulk* medium, the azimuth rotation is also a sinusoidal function of 2φ . The amplitude Δ_1 and the offset Δ_2 are largely controlled by the anisotropy and chirality of the bulk medium, respectively.²⁵

The optical rotation and circular dichroism (CD) spectra of the bulk medium are not independent but are closely connected by Kramers-Kronig relations.²⁶ For metal nanoparticle assemblies, this interrelationship is not yet thoroughly studied. Drachev *et al.*²⁷ observed large local CD in fractal aggregates of silver nanoparticles by means of photon scanning tunneling microscopy. The value of CD averaged over the whole sample was close to zero. Yannopoulos²⁸ noted that interacting nanospheres occupying the sites of a rectangular lattice show a considerable CD around the surface plasmon frequency. This planar nonchiral structure is indeed extrinsically chiral.²⁹ Fan and Govorov^{30,31} showed that the helical arrangements of gold

nanoparticles exhibit CD in the visible wavelength range. It is noteworthy that chiral molecules and biomolecules show strong CD in the UV range. Circular dichroism of metallic nanoparticle assemblies originates in the electromagnetic dipole-dipole interaction between particles. Recently Kuzyk *et al.*³² used DNA origami to create left- and right-handed nanohelices of diameter 34 nm and helical pitch 57 nm, by nine gold nanoparticles of radius 5 nm.

Inspired by the work of Sepúlveda *et al.*²³ and Fan and Govorov,^{30,31} we study CD of interacting metallic nanoparticles subject to an external static *magnetic field*. We find that the simplest *achiral* cluster, a dimer, exhibits CD in the presence of the magnetic field. Near the surface plasmon frequency, CD increases considerably. Quite remarkably, CD depends on the directions of the magnetic field \mathbf{B} and the light wave vector \mathbf{k} with respect to the dimer axis \mathbf{n} . In particular, CD vanishes if (i) $\mathbf{k} \parallel \mathbf{n}$ and $\mathbf{B} \perp \mathbf{n}$, (ii) $\mathbf{k} \perp \mathbf{n}$ and $\mathbf{B} \parallel \mathbf{n}$, and (iii) $\mathbf{k} \perp \mathbf{n}$, $\mathbf{B} \perp \mathbf{n}$, and $\mathbf{k} \perp \mathbf{B}$. This reminds us of the intriguing magnetochiral dichroism^{33–37} of a solution of chiral molecules: the absorption of a light beam parallel to the magnetic field and a beam antiparallel to the field are slightly different. Indeed, on the basis of symmetry arguments, it has been shown³⁸ that the dielectric tensor of a chiral medium has a term proportional to $\mathbf{k} \cdot \mathbf{B}$.

Our article is organized as follows. In Sec. II we introduce the model. The circular dichroism and Faraday rotation spectra of a dimer, a set of nanoparticles positioned on a helix, and a random gas of nanoparticles are presented in Secs. III, IV, and V, respectively. A summary of our results and discussions is given in Sec. VI.

II. MODEL

A. Polarizability tensor of the nanoparticle

We adopt the free electron Drude model to describe the magneto-optical response of *bulk* metals. For an electron subject to the static magnetic field $\mathbf{B} = B(b_x, b_y, b_z)$ and the oscillating electric field $\mathbf{E}(t) = \text{Re}[\mathbf{E}(\omega)\exp(-i\omega t)]$ of the light, the equation of motion reads

$$m_e \frac{d^2 \mathbf{x}}{dt^2} = -m_e \gamma \frac{d\mathbf{x}}{dt} - e \left(\mathbf{E}(t) + \frac{1}{c} \frac{d\mathbf{x}}{dt} \times \mathbf{B} \right). \quad (3)$$

Here \mathbf{x} , γ , m_e , and $-e < 0$ denote the displacement vector, relaxation constant, effective mass, and charge of the electron, respectively. cgs units are used throughout this paper.

The polarization of the medium is $\mathbf{P}(t) = -en_e \mathbf{x}(t)$, where n_e is the number of conduction electrons per unit volume. Solving Eq. (3) with the ansatz $\mathbf{x}(t) = \text{Re}[\mathbf{x}(\omega)\exp(-i\omega t)]$ yields $\mathbf{P}(\omega) = -en_e \mathbf{x}(\omega) = \chi(\omega)\mathbf{E}(\omega)$. For weak magnetic fields (about 10^4 G), the cyclotron frequency

$$\omega_c = \frac{eB}{m_e c} \quad (4)$$

is much smaller than the light frequency ω . Thus we calculate the electric susceptibility tensor $\chi(\omega)$ and the permittivity tensor $\epsilon(\omega) = \mathbf{I} + 4\pi\chi(\omega)$ to first order in ω_c/ω . Indeed,

$$\epsilon(\omega) = \begin{pmatrix} \epsilon_{xx}(\omega) & iG\omega_c b_z & -iG\omega_c b_y \\ -iG\omega_c b_z & \epsilon_{yy}(\omega) & iG\omega_c b_x \\ iG\omega_c b_y & -iG\omega_c b_x & \epsilon_{zz}(\omega) \end{pmatrix}, \quad (5)$$

where $\epsilon_{xx} = \epsilon_{yy} = \epsilon_{zz} = 1 - \omega_p^2/(\omega^2 + i\gamma\omega)$, $G = \omega_p^2/(\omega^2 + i\gamma\omega)^2$, and $\omega_p = \sqrt{4\pi n_e e^2/m_e}$ is the plasma frequency.

Now we consider a metal nanoparticle of radius a much smaller than the light wavelength. The polarizability tensor of the spherical nanoparticle is³⁹

$$\alpha(\omega) = a^3(\epsilon - \epsilon_m \mathbf{I})(\epsilon + 2\epsilon_m \mathbf{I})^{-1}, \quad (6)$$

where ϵ_m is the dielectric constant of the isotropic host medium and \mathbf{I} is the identity matrix. To first order in ω_c/ω ,

$$\alpha(\omega) = \begin{pmatrix} \alpha_{xx}(\omega) & -\mathcal{F}\omega_c b_z & \mathcal{F}\omega_c b_y \\ \mathcal{F}\omega_c b_z & \alpha_{yy}(\omega) & -\mathcal{F}\omega_c b_x \\ -\mathcal{F}\omega_c b_y & \mathcal{F}\omega_c b_x & \alpha_{zz}(\omega) \end{pmatrix}, \quad (7)$$

where $\alpha_{xx} = \alpha_{yy} = \alpha_{zz} = a^3(\epsilon_{xx} - \epsilon_m)/(\epsilon_{xx} + 2\epsilon_m)$ and

$$\mathcal{F} = -3ia^3 \frac{\omega_p^2}{\omega(\omega + i\gamma)^2} \frac{\epsilon_m}{(\epsilon_{xx} + 2\epsilon_m)^2}. \quad (8)$$

The off-diagonal terms of α which are proportional to the magnetic field B might seem small at first glance. However, the factor \mathcal{F} becomes considerably large at frequencies where $\text{Re}(\epsilon_{xx} + 2\epsilon_m) = \pm \text{Im}(\epsilon_{xx})$. These frequencies are near to the surface plasmon frequency where $\text{Re}(\epsilon_{xx} + 2\epsilon_m) = 0$.

The simple Drude model helps us to understand the origin of plasmon-induced magneto-optical activity of noble metal clusters.²³ To make a better link to experiments, we use the Drude critical points model⁴⁰ for the dielectric function of *bulk* Ag and Au. This model well reproduces the experimental data of Johnson and Christy.⁴¹ We also modify the dielectric function of bulk metal to take into account the finite size effects in small metallic spheres. We rely on the following radius-dependent dielectric function⁴²

$$\epsilon_{xx}(\omega) = \epsilon_{xx}^{\text{bulk}}(\omega) + \frac{\omega_p^2}{\omega^2 + i\gamma_{\text{bulk}}\omega} - \frac{\omega_p^2}{\omega^2 + i\gamma\omega}, \quad (9)$$

where $\gamma = \gamma_{\text{bulk}} + Av_F/a$ is the radius-dependent relaxation, v_F is the Fermi velocity, and the parameter A is of order 1. To calculate the size-corrected α_{xx} and \mathcal{F} , we assume that $A = 3/4$,⁴³ although there is a slight disagreement among authors about A .^{42–45} For silver, $\omega_p = 1.386 \times 10^{16} \text{ s}^{-1}$, $\gamma_{\text{bulk}} = 4.584 \times 10^{13} \text{ s}^{-1}$, and $v_F = 1.39 \times 10^8 \text{ cm/s}$. For gold, $\omega_p = 1.32 \times 10^{16} \text{ s}^{-1}$, $\gamma_{\text{bulk}} = 1.08 \times 10^{14} \text{ s}^{-1}$, and $v_F = 1.4 \times 10^8 \text{ cm/s}$.

B. Coupled-dipole equations

To describe interaction of an incident electromagnetic wave with a set of N identical particles, we use the dipole approximation: Each metal nanoparticle of radius a behaves as a point dipole with polarizability tensor α . The local field acting on any dipole is a superposition of the incident field and secondary fields produced by other dipoles. Thus the coupled-dipole equations (CDEs) for the induced dipoles are

$$\mathbf{d}_i(\omega) = \alpha(\omega) \left(\mathbf{E}(\mathbf{r}_i, \omega) + \sum_{j=1}^N \mathbf{W}(\mathbf{r}_i - \mathbf{r}_j) \cdot \mathbf{d}_j(\omega) \right). \quad (10)$$

Here \mathbf{r}_i and $\text{Re}[\mathbf{d}_i(\omega)\exp(-i\omega t)]$ denote the position and light-induced dipole of the i th particle, respectively. The

dyadic Green's function \mathbf{W} determines the field produced by the oscillating dipole,⁴⁶

$$W_{\alpha,\beta}(\mathbf{r}_{ij}) = \left[(1 - ik|\mathbf{r}_{ij}|) \left(\frac{3(\mathbf{r}_{ij})_\alpha(\mathbf{r}_{ij})_\beta - |\mathbf{r}_{ij}|^2\delta_{\alpha\beta}}{\epsilon_m|\mathbf{r}_{ij}|^5} \right) + k^2 \left(\frac{|\mathbf{r}_{ij}|^2\delta_{\alpha\beta} - (\mathbf{r}_{ij})_\alpha(\mathbf{r}_{ij})_\beta}{\epsilon_m|\mathbf{r}_{ij}|^3} \right) \right] e^{ik|\mathbf{r}_{ij}|}, \quad (11)$$

where $\mathbf{r}_{ij} = \mathbf{r}_i - \mathbf{r}_j$, $k = \omega\sqrt{\epsilon_m}/c$, and the Greek subscripts denote the Cartesian components. The coupled-dipole equations are widely used to describe the optical properties of nanoparticle clusters; see, for example, Refs. 47–51.

III. DIMER

A. Circular dichroism

It is instructive to consider a dimer as the simplest *achiral* cluster. We assume that the particles reside at $\mathbf{r}_1 = (0,0,0)$ and $\mathbf{r}_2 = (L,0,0)$ [see Fig. 1(a)]. The vector $\mathbf{n} = (\mathbf{r}_2 - \mathbf{r}_1)/L$ specifies the axis of the dimer. The dimer interacts with the electromagnetic field $\mathbf{E}(\mathbf{r},\omega) = E_0\mathbf{e} \exp(i\mathbf{k} \cdot \mathbf{r})$. The polarization vector \mathbf{e} and the wave vector $\mathbf{k} = k(\sin\theta \cos\varphi, \sin\theta \sin\varphi, \cos\theta)$ are perpendicular.

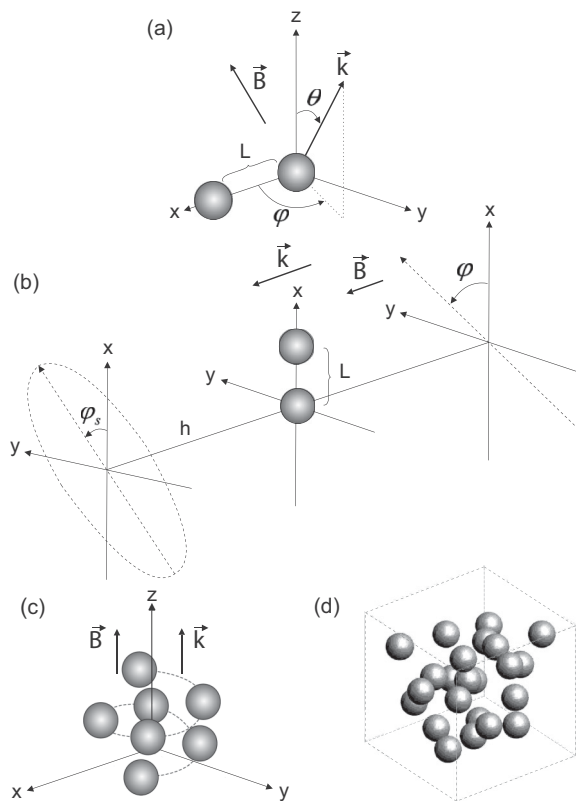


FIG. 1. (a) Schematics of a dimer subject to the magnetic field $\mathbf{B} = B(b_x, b_y, b_z)$. The incident light propagates in the direction $\mathbf{k} = k(\sin\theta \cos\varphi, \sin\theta \sin\varphi, \cos\theta)$. (b) A dimer interacts with a linearly polarized light with polarization azimuth φ . At the point $(0,0,h)$, the scattered wave is elliptically polarized and the polarization azimuth is φ_s . Here $\mathbf{k} \parallel \mathbf{B} \parallel \hat{z}$. (c) Helical arrangement of nanoparticles. Here $\mathbf{k} \parallel \mathbf{B} \parallel \hat{z}$. (d) Part of a random arrangement of nanoparticles.

The light-induced dipole moments obey the equations $\mathbf{d}_1 = \alpha(\mathbf{E}(\mathbf{r}_1,\omega) + \mathbf{W} \cdot \mathbf{d}_2)$ and $\mathbf{d}_2 = \alpha(\mathbf{E}(\mathbf{r}_2,\omega) + \mathbf{W} \cdot \mathbf{d}_1)$. Here

$$\mathbf{W} = \begin{pmatrix} \eta + \xi & 0 & 0 \\ 0 & \eta & 0 \\ 0 & 0 & \eta \end{pmatrix}, \quad (12)$$

$$\eta(L,k) = \left(k^2 - \frac{1}{L^2} + \frac{ik}{L} \right) \frac{e^{ikL}}{\epsilon_m L},$$

$$\xi(L,k) = \left(-k^2 + \frac{3}{L^2} - \frac{3ik}{L} \right) \frac{e^{ikL}}{\epsilon_m L}.$$

By introducing $\mathbf{d}_m = \alpha^{-1}(\mathbf{d}_1 - \mathbf{d}_2)$, $\mathbf{d}_p = \alpha^{-1}(\mathbf{d}_1 + \mathbf{d}_2)$, $\mathbf{E}_m = \mathbf{E}(\mathbf{r}_1,\omega) - \mathbf{E}(\mathbf{r}_2,\omega)$, and $\mathbf{E}_p = \mathbf{E}(\mathbf{r}_1,\omega) + \mathbf{E}(\mathbf{r}_2,\omega)$, the coupled-dipole equations can be written as

$$(\mathbf{I} + \mathbf{W}\alpha)\mathbf{d}_m = \mathbf{E}_m, \quad (13)$$

$$(\mathbf{I} - \mathbf{W}\alpha)\mathbf{d}_p = \mathbf{E}_p,$$

which are easily solvable. To first order in ω_c/ω ,

$$\mathbf{d}_{mx} = \frac{(1 + \eta\alpha_{xx})E_{mx} - (\eta + \xi)\alpha_{xy}E_{my} - (\eta + \xi)\alpha_{xz}E_{mz}}{(1 + \eta\alpha_{xx})(1 + (\eta + \xi)\alpha_{xx})},$$

$$\mathbf{d}_{my} = \frac{1}{1 + \eta\alpha_{xx}} \left(\frac{\eta\alpha_{xy}E_{mx}}{1 + (\eta + \xi)\alpha_{xx}} + E_{my} - \frac{\eta\alpha_{yz}E_{mz}}{1 + \eta\alpha_{xx}} \right),$$

$$\mathbf{d}_{mz} = \frac{1}{1 + \eta\alpha_{xx}} \left(\frac{\eta\alpha_{xz}E_{mx}}{1 + (\eta + \xi)\alpha_{xx}} + \frac{\eta\alpha_{yz}E_{my}}{1 + \eta\alpha_{xx}} + E_{mz} \right),$$

$$\mathbf{d}_{px} = \frac{(1 - \eta\alpha_{xx})E_{px} + (\eta + \xi)\alpha_{xy}E_{py} + (\eta + \xi)\alpha_{xz}E_{pz}}{(1 - \eta\alpha_{xx})(1 - (\eta + \xi)\alpha_{xx})},$$

$$\mathbf{d}_{py} = \frac{1}{1 - \eta\alpha_{xx}} \left(-\frac{\eta\alpha_{xy}E_{px}}{1 - (\eta + \xi)\alpha_{xx}} + E_{py} + \frac{\eta\alpha_{yz}E_{pz}}{1 - \eta\alpha_{xx}} \right),$$

$$\mathbf{d}_{pz} = \frac{1}{1 - \eta\alpha_{xx}} \left(-\frac{\eta\alpha_{xz}E_{px}}{1 - (\eta + \xi)\alpha_{xx}} - \frac{\eta\alpha_{yz}E_{py}}{1 - \eta\alpha_{xx}} + E_{pz} \right). \quad (14)$$

The absorption cross section of the dimer can be expressed in terms of the auxiliary variables \mathbf{d}_m and \mathbf{d}_p . Indeed,

$$\sigma = \frac{4\pi}{E_0^2\sqrt{\epsilon_m}} \frac{\omega}{c} \text{Im}(\alpha^{-1*} \mathbf{d}_1^* \cdot \mathbf{d}_1 + \alpha^{-1*} \mathbf{d}_2^* \cdot \mathbf{d}_2),$$

$$= \frac{2\pi}{E_0^2\sqrt{\epsilon_m}} \frac{\omega}{c} \text{Im}(\alpha \mathbf{d}_m \cdot \mathbf{d}_m^* + \alpha \mathbf{d}_p \cdot \mathbf{d}_p^*). \quad (15)$$

We pay attention to the absorption cross sections σ_{\pm} corresponding to the polarization vectors

$$\mathbf{e}_{\pm} = \frac{1}{\sqrt{2}} (\cos\theta \cos\varphi \mp i \sin\varphi, \cos\theta \sin\varphi \pm i \cos\varphi, -\sin\theta). \quad (16)$$

\mathbf{e}_+ and \mathbf{e}_- describe the right and left circularly polarized light, respectively. A straightforward but lengthy calculation shows that the dimer is circular dichroic:

$$\sigma_+ - \sigma_- = \omega_c(k_x b_x \Lambda_1(\eta, \xi) + (k_y b_y + k_z b_z) \Lambda_2(\eta, \xi)) k_x^2 L^2 + \omega_c(k_x b_x \Lambda_1(-\eta, -\xi) + (k_y b_y + k_z b_z) \times \Lambda_2(-\eta, -\xi)) (4 + k_x^2 L^2), \quad (17)$$

where

$$\begin{aligned}\Lambda_1(\eta, \xi) &= -\frac{4\pi}{\varepsilon_m |1 + \eta\alpha_{xx}|^2} \\ &\times \left[\text{Re}(\mathcal{F}) + \text{Im} \left(\frac{2\eta\mathcal{F}}{1 + \eta\alpha_{xx}} \right) \text{Im}(\alpha_{xx}) \right], \\ \Lambda_2(\eta, \xi) &= \frac{4\pi}{\varepsilon_m |1 + \eta\alpha_{xx}|^2} \left[-\text{Re} \left(\frac{1 + \eta\alpha_{xx}}{1 + (\eta + \xi)\alpha_{xx}} \right) \text{Re}(\mathcal{F}) \right. \\ &\quad + \text{Im} \left(\frac{(1 + \eta\alpha_{xx})(\eta^* + \xi^*)\mathcal{F}^*}{|1 + (\eta + \xi)\alpha_{xx}|^2} \right. \\ &\quad \left. \left. - \frac{\eta\mathcal{F}}{1 + (\eta + \xi)\alpha_{xx}} \right) \text{Im}(\alpha_{xx}) \right].\end{aligned}\quad (18)$$

As expected, the achiral dimer exhibits no circular dichroism in the absence of the external magnetic field ($\omega_c = 0$). Quite remarkably, $\sigma_+ - \sigma_-$ depends on the directions of the magnetic field $\mathbf{B} = B(b_x, b_y, b_z)$ and the wave vector $\mathbf{k} = (k_x, k_y, k_z)$ with respect to the dimer axis \mathbf{n} [see Figs. 1(a) and 2]. The circular dichroism certainly vanishes if (i) $\mathbf{k} \parallel \mathbf{n}$ and $\mathbf{B} \perp \mathbf{n}$, (ii) $\mathbf{k} \perp \mathbf{n}$ and $\mathbf{B} \parallel \mathbf{n}$, and (iii) $\mathbf{k} \perp \mathbf{n}$, $\mathbf{B} \perp \mathbf{n}$, and $\mathbf{k} \perp \mathbf{B}$.

Note that $\Lambda_1 \propto \mathcal{F}$ and $\Lambda_2 \propto \mathcal{F}$. Near the surface plasmon frequency, \mathcal{F} and hence $\sigma_+ - \sigma_-$ increase considerably. Moreover, one may expect enhanced circular dichroism where $\text{Re}(1 \pm \eta\alpha_{xx}) = 0$ or $\text{Re}(1 \pm (\eta + \xi)\alpha_{xx}) = 0$. We found that these resonances hardly occur for interparticle distance $L > 3a$. Note that the dipole approximation is not reliable in the region $L < 3a$.

Figure 2 exemplifies $\sigma_+ - \sigma_-$ of an Ag dimer for various directions of \mathbf{B} and \mathbf{k} . Here $a = 10$ nm, $L = 3a$, and $B = 8000$ G. For $\mathbf{k} \parallel (0, 0, 1)$ and $\mathbf{B} \parallel (1, 0, 0)$ the dimer exhibits no circular dichroism, but upon light propagation along $\mathbf{k} \parallel (0.5, 0, 0.866)$ the dimer responds quite differently. Considering the case $\mathbf{k} \parallel (0, 0, 1)$ and $\mathbf{B} \parallel (0, 0, 1)$, we find that the peaks of $\sigma_+ - \sigma_-$ may increase and shift as the direction of the magnetic field varies.

Figure 3 demonstrates the circular dichroism $\sigma_+ - \sigma_-$ in units of the geometric cross section πa^2 as a function of

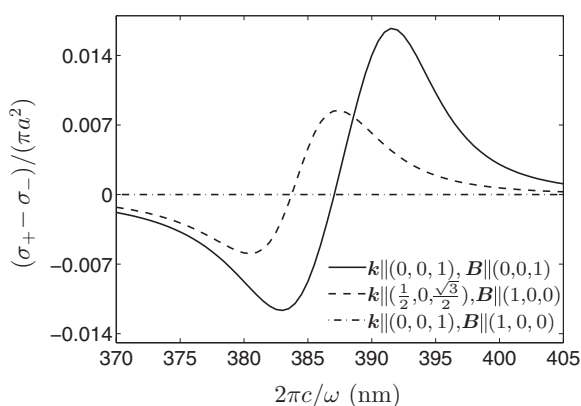


FIG. 2. $(\sigma_+ - \sigma_-)/(\pi a^2)$ of an Ag dimer as a function of the wavelength $2\pi c/\omega$ for various directions of \mathbf{B} and \mathbf{k} . Here $a = 10$ nm, $L = 3a$, $\varepsilon_m = 1.7$, and $B = 8000$ G.

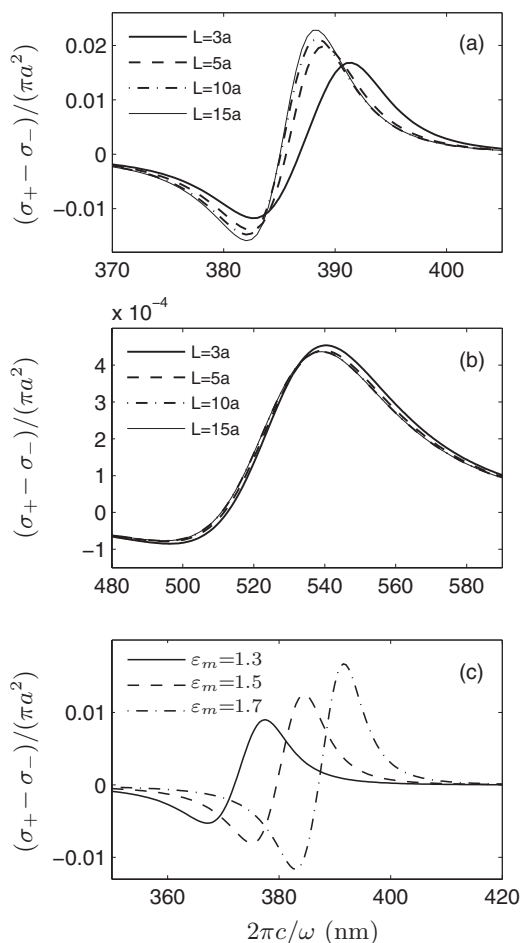


FIG. 3. $(\sigma_+ - \sigma_-)/(\pi a^2)$ as a function of the wavelength $2\pi c/\omega$ for (a) Ag dimer in a medium with $\varepsilon_m = 1.7$, (b) Au dimer in a medium with $\varepsilon_m = 1.7$, and (c) Ag dimer with interparticle distance $L = 3a$. Here $a = 10$ nm, $\mathbf{k} \parallel \hat{z}$, and $\mathbf{B} = 8000$ G \hat{z} .

the wavelength $2\pi c/\omega$. Here $a = 10$ nm, $\mathbf{k} \parallel \hat{z}$, and $\mathbf{B} = 8000$ G \hat{z} . An Ag dimer exhibits a considerable negative (positive) dichroism at wavelength $2\pi c/\omega = 383$ nm (391.5 nm) when $L = 3a$ and $\varepsilon_m = 1.7$ see [Fig. 3(a)]. These peaks increase and slightly shift to lower wavelengths as L increases. The spectrum does not change significantly upon increasing the interparticle distance beyond $L = 15a$, since the dipolar interaction becomes quite weak. In the same host medium, the dichroism of an Au dimer reaches its maximum at wavelength $2\pi c/\omega = 540$ nm [see Fig. 3(b)]. The dichroism of Ag dimer is about 20 times stronger than that of Au dimer. This is expected, as $1/\text{Im}(\varepsilon_{xx})$ and hence \mathcal{F} of Ag is greater than that of Au. Figure 3(c) shows the impact of the host medium on the circular dichroism spectrum of the Ag dimer. Both peaks of the spectrum grow and shift to higher wavelengths as ε_m increases.

B. Faraday rotation

Now we assume that the dimer interacts with a linearly polarized light with the polarization vector

$$\mathbf{e} = (\cos \varphi, \sin \varphi, 0). \quad (19)$$

The wave vector \mathbf{k} and the external magnetic field \mathbf{B} are along the unit vector $\hat{\mathbf{z}}$. We measure the electric field \mathbf{E}_s radiated by the dimer at $(0,0,h)$, where $h \gg L > a$ [see Fig. 1(b)]. In the far (radiation) zone the scattered field takes on the form

$$\begin{aligned} \mathbf{E}_s &= (\mathbf{d}_1 - \hat{\mathbf{z}}\hat{\mathbf{z}} \cdot \mathbf{d}_1) \frac{k^2 e^{ikh}}{\varepsilon_m h} + (\mathbf{d}_2 - \hat{\mathbf{z}}\hat{\mathbf{z}} \cdot \mathbf{d}_2) \frac{k^2 e^{ikh}}{\varepsilon_m h}, \\ &= (\boldsymbol{\alpha} \mathbf{d}_p - \hat{\mathbf{z}}\hat{\mathbf{z}} \cdot \boldsymbol{\alpha} \mathbf{d}_p) \frac{k^2 e^{ikh}}{\varepsilon_m h}. \end{aligned} \quad (20)$$

The electromagnetic wave $\mathbf{E}_s = (E_{sx}, E_{sy}, 0)$ is elliptically polarized. The vibration ellipse can be characterized by its azimuth φ_s , the angle between the semimajor axis and the unit vector $\hat{\mathbf{x}}$, and its ellipticity $\tan \mu$, the ratio of the length of its semiminor axis to that of its semimajor axis. Operationally defined in terms of measurable intensities, the Stokes parameters^{52,53}

$$\begin{aligned} I &= |E_{sx}|^2 + |E_{sy}|^2, \\ Q &= |E_{sx}|^2 - |E_{sy}|^2, \\ U &= 2\text{Re}(E_{sx}^* E_{sy}), \\ V &= 2\text{Im}(E_{sx}^* E_{sy}), \end{aligned} \quad (21)$$

determine completely the state of polarization. Indeed,

$$\begin{aligned} \varphi_s &= \frac{1}{2} \arctan \frac{U}{Q}, \\ \mu &= \frac{1}{2} \arcsin \frac{V}{I}. \end{aligned} \quad (22)$$

Note that the azimuth and the ellipticity angle of the linearly polarized incident wave are φ and 0, respectively. Hereafter we focus on the polarization azimuth rotation $\varphi_s - \varphi$ and the ellipticity angle variation μ .

Powered by the analytical expressions (14) and (20), we find that to first order in ω_c/ω ,

$$\begin{aligned} \varphi_s - \varphi &= \frac{1}{2} \arctan \left(\frac{J_1 \sin 2\varphi}{\cos 2\varphi + J_2} \right) - \varphi \\ &+ \frac{\omega_c}{2} \frac{J_1 J_3 \sin^2 2\varphi + (J_3 \cos 2\varphi + J_4)(\cos 2\varphi + J_2)}{(J_1 \sin 2\varphi)^2 + (\cos 2\varphi + J_2)^2}, \\ \mu &= \frac{1}{2} \arcsin \left(\frac{-J_5 \sin 2\varphi}{J_2 \cos 2\varphi + 1} \right) \\ &+ \frac{\omega_c}{2} \frac{(J_6 \cos 2\varphi + J_7)(J_2 \cos 2\varphi + 1) - J_4 J_5 \sin^2 2\varphi}{(J_2 \cos 2\varphi + 1) \sqrt{(J_2 \cos 2\varphi + 1)^2 - (J_5 \sin 2\varphi)^2}}, \end{aligned} \quad (23)$$

where the parameters J_1 – J_7 are reported in the Appendix. As already mentioned in the Introduction, the polarization azimuth rotation is composed of two terms which are different in nature. The first term of $\Delta = \varphi_s - \varphi$, which does not depend on the external magnetic field, is the structural polarization azimuth rotation $\Delta_{\text{str}}(\varphi)$. Note that a dimer is an anisotropic and achiral object. By switching off the dipolar interaction between the spheres ($\eta, \xi \rightarrow 0$), this structural azimuth rotation expectedly vanishes. The second term of $\varphi_s - \varphi$, which is proportional to the external magnetic field, is the Faraday rotation $B\Delta_{\text{Far}}(\varphi)$. Note that $J_3 \propto \mathcal{F}$ and $J_4 \propto \mathcal{F}$; thus the plasmon resonance boosts the Faraday rotation. Similarly, the first term of μ describes the structural ellipticity angle

variation. J_4 , J_6 , and J_7 are proportional to \mathcal{F} . The plasmon excitation thus enhances the second term of μ , which is the Faraday ellipticity.

We have numerically studied J_1 – J_7 . We find that in a large domain of parameter space,

$$\begin{aligned} J_1 &\simeq 1, \quad J_2 \ll 1, \quad J_3 \omega_c \ll 1, \quad J_4 \omega_c \ll 1, \\ J_5 &\ll 1, \quad J_6 \omega_c \ll 1, \quad J_7 \omega_c \ll 1, \end{aligned} \quad (24)$$

which allows us to rewrite Eq. (23) as

$$\begin{aligned} \varphi_s - \varphi &\simeq -\frac{J_2}{2} \sin 2\varphi + \frac{\omega_c}{2} ((J_4 - J_2 J_3) \cos 2\varphi + J_3), \\ \mu &\simeq -\frac{J_5}{2} \sin 2\varphi + \frac{\omega_c}{2} (-J_7 J_2 \cos 2\varphi + J_7). \end{aligned} \quad (25)$$

In other words, provided that condition (24) is satisfied, Δ_{str} , $B\Delta_{\text{Far}}$, μ_{str} , and $B\mu_{\text{Far}}$ are a sinusoidal function of 2φ . These functions can be represented in the form of Eq. (2). For a dimer $\Delta_2 = 0$ and $\mu_2 = 0$.

Now we use Eq. (23) to access the structural polarization azimuth rotation Δ_{str} of a silver dimer as a function of φ and $2\pi c/\omega$. We assume that $a = 10$ nm, $L = 3a$, $\varepsilon_m = 1.7$, and $B = 0$. Figure 4(a) shows that Δ_{str} is a sinusoidal function of 2φ . At wavelength 420 nm, Δ_{str} has a considerable amplitude of 7.84° . Upon increasing the wavelength to 500 nm, the

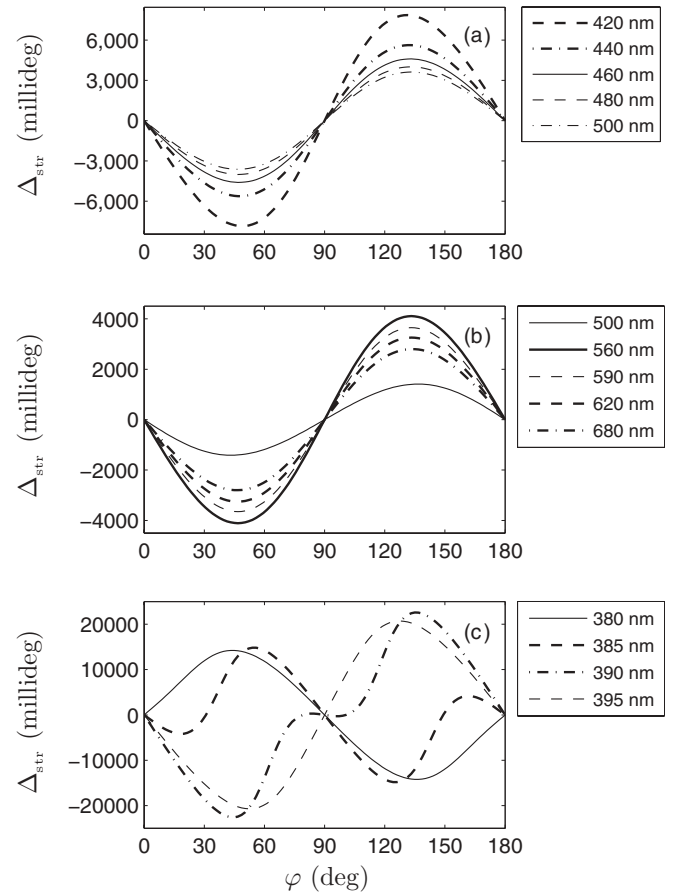


FIG. 4. $\Delta_{\text{str}}(\varphi)$ of (a) Ag dimer, (b) Au dimer, and (c) Ag dimer as a function of φ for various wavelengths $2\pi c/\omega$. Here $a = 10$ nm, $L = 3a$, $\varepsilon_m = 1.7$, and $B = 0$.

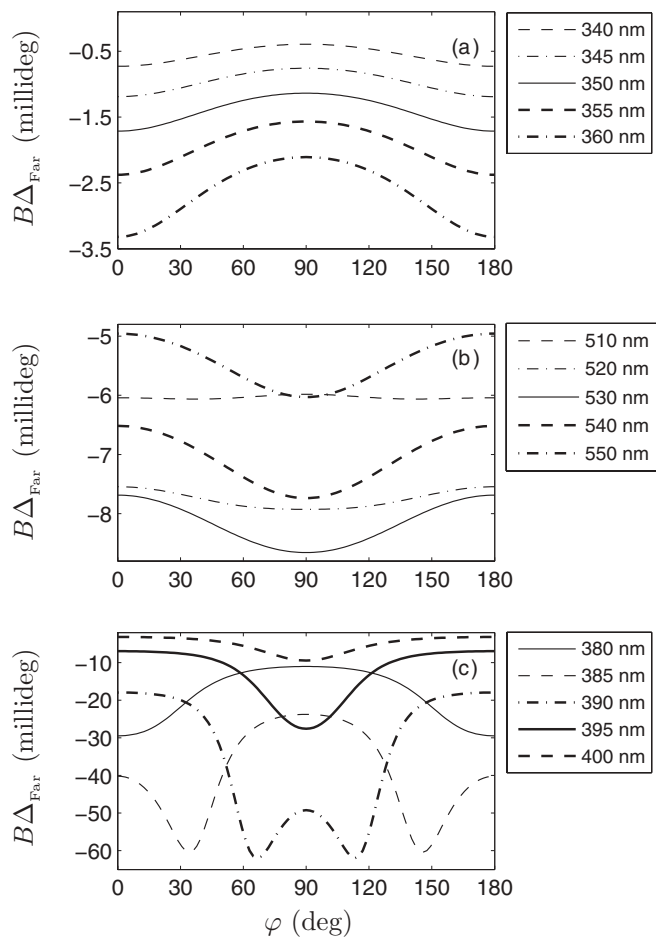


FIG. 5. $B\Delta_{\text{Far}}(\varphi)$ of (a) Ag dimer, (b) Au dimer, and (c) Ag dimer as a function of φ for various wavelengths $2\pi c/\omega$. Here $a = 10$ nm, $L = 3a$, $\varepsilon_m = 1.7$, and $B = 8000$ G.

amplitude decreases to 3.62° . Figure 4(b) shows a similar plot for a gold dimer. Here Δ_{str} is less than 4.1° . Figure 4(c) shows that in the narrow window $380 \leq 2\pi c/\omega \leq 395$ nm, Δ_{str} of a silver dimer is a nonsinusoidal function. This is because the condition (24) is violated. Quite remarkably, in this window Δ_{str} can be as large as 22.6° . Figures 5(a) and 5(b) show the Faraday rotation of a silver and a gold dimer subject to the magnetic field $B = 8000$ G, respectively. $B\Delta_{\text{Far}}(\varphi)$ is a sinusoidal function of 2φ . Apparently the maximum of the Faraday rotation $<0.01^\circ$ is much less than the maximum of structural azimuth rotation 7.84° . Figure 5(c) shows that in the narrow window 380–400 nm, $B\Delta_{\text{Far}}(\varphi)$ of a silver dimer is a nonsinusoidal function.

The structural ellipticity angle variation μ_{str} behaves similar to Δ_{str} . The sinusoidal μ_{str} of a silver (gold) dimer gains its maximum 0.1° (3.3°) at wavelength 480 nm (510 nm). In the window 380–395 nm, μ_{str} of a silver dimer is a nonsinusoidal function [see Fig. 6(a)]. For the magnetic field $B = 8000$ G and wavelengths not in the window 330–440 nm (540–556 nm), $B\mu_{\text{Far}}$ of a silver (gold) dimer is a sinusoidal function of 2φ . In this regime, the maximum of Faraday ellipticity angle variation 0.004° (0.0046°) of a silver (gold) dimer is much less than the maximum of structural ellipticity angle variation 0.1° (3.3°). The nonsinusoidal behaviors of $B\mu_{\text{Far}}$

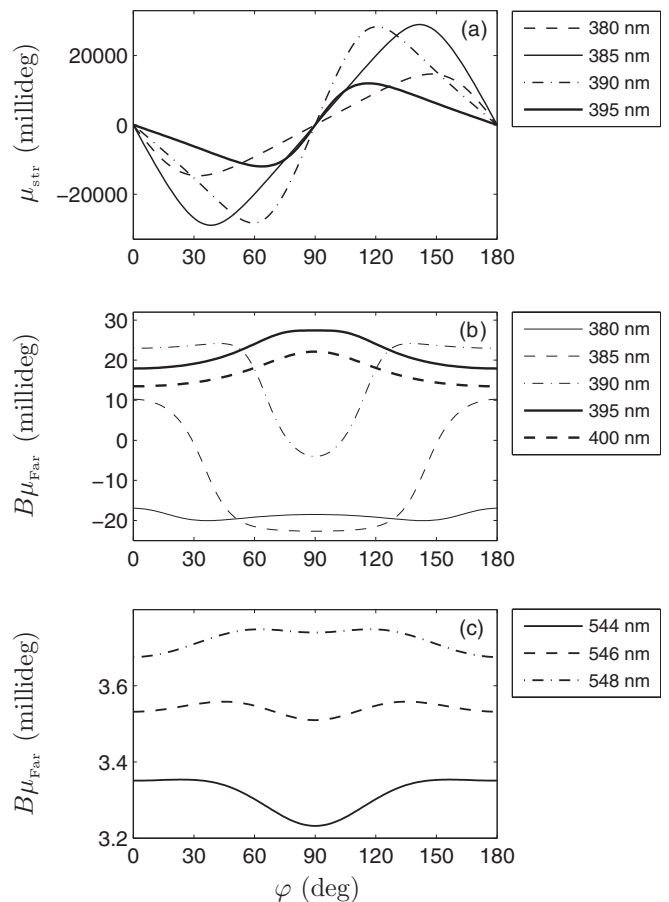


FIG. 6. (a) $\mu_{\text{str}}(\varphi)$ of Ag dimer, (b) $B\mu_{\text{Far}}(\varphi)$ of Ag dimer, and (c) $B\mu_{\text{Far}}(\varphi)$ of Au dimer as a function of φ for various wavelengths $2\pi c/\omega$. Here $a = 10$ nm, $L = 3a$, $\varepsilon_m = 1.7$, and $B = 8000$ G.

for silver and gold dimer are shown in Figs. 6(b) and 6(c), respectively.

IV. NANOPARTICLES POSITIONED ON A HELIX

Fan and Govorov^{30,31} studied circular dichroism of a set of nanoparticles positioned on a helix. They did not investigate the effect of an external static magnetic field. We aim to further study correlation between the chirality and the magneto-optical response of a set of N identical nanoparticles of radius a . We assume that the i th particle resides at

$$\begin{aligned} x_i &= R_{\text{helix}} \cos(i\theta_{\text{helix}} - \theta_{\text{helix}}), \\ y_i &= R_{\text{helix}} \sin(i\theta_{\text{helix}} - \theta_{\text{helix}}), \\ z_i &= (i - 1)p_{\text{helix}}\theta_{\text{helix}}/(2\pi). \end{aligned} \quad (26)$$

As an example, we choose $N = 15$, $a = 10$ nm, $R_{\text{helix}} = 30$ nm, $p_{\text{helix}} = 30$ nm, and $\theta_{\text{helix}} = \pi/3$.

We assume that the helical structure interacts with the electromagnetic field $\mathbf{E}(\mathbf{r}, \omega) = E_0 \mathbf{e} \exp(i\mathbf{k} \cdot \mathbf{r})$. We compute the absorption cross sections σ_{\pm} corresponding to the polarization vectors \mathbf{e}_{\pm} introduced in Eq. (16). The dielectric constant of the matrix $\varepsilon_m = 1.7$ and the external magnetic field $B = 0$. Figure 7(a) delineates $\sigma_{+} - \sigma_{-}$ of a helical assembly of silver nanoparticles as a function of wavelength $2\pi c/\omega$ for various

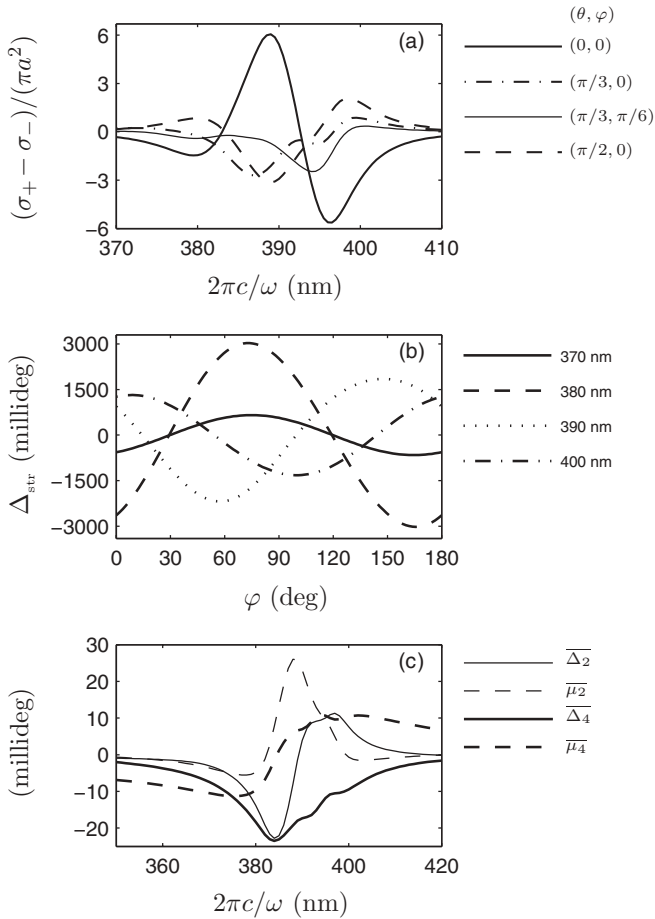


FIG. 7. Magneto-optical response of 15 silver nanoparticles positioned on a helix, $a = 10$ nm and $\varepsilon_m = 1.7$. (a) $(\sigma_+ - \sigma_-)/(\pi a^2)$ as a function of $2\pi c/\omega$, for various directions of $\mathbf{k} = k(\sin\theta \cos\varphi, \sin\theta \sin\varphi, \cos\theta)$. Here $B = 0$. (b) Δ_{str} as a function of φ , for various wavelengths $2\pi c/\omega$. (c) $\overline{\Delta_2}$, $\overline{\mu_2}$, $\overline{\Delta_4}$, and $\overline{\mu_4}$ as a function of $2\pi c/\omega$. Here $B = 8000$ G.

directions of $\mathbf{k} = k(\sin\theta \cos\varphi, \sin\theta \sin\varphi, \cos\theta)$. We can see that the CD spectrum has both positive and negative bands. The peaks of the CD spectrum change and shift as the direction of light wave vector \mathbf{k} varies. For light propagation along the helix axis, i.e., $\mathbf{k} \parallel \hat{z}$, $\sigma_+ - \sigma_-$ gains its considerable extrema $6.05\pi a^2$ and $-5.63\pi a^2$ at wavelengths 389 and 396 nm, respectively. We also find that⁵⁴ the CD spectrum does not change significantly as the static magnetic field increases to $B = 8000$ G. We observe that the CD spectrum is quite susceptible to neglect of finite-size effects in small metallic spheres [see Eq. (9)]. This point is overlooked in Ref. 30.

We now assume that $\mathbf{k} \parallel \hat{z}$, $\mathbf{B} \parallel \hat{z}$, and the helical structure interacts with a linearly polarized light with the polarization vector introduced in Eq. (19) [see Fig. 1(c)]. Direct numerical solution of the coupled-dipole equations (10) allows us to obtain the azimuth φ_s and ellipticity angle μ which characterize the vibration ellipse of the scattered field. Figure 7(b) shows the structural polarization azimuth rotation $\Delta_{\text{str}}(\varphi)$ of a helical structure as a function of φ . We observe that Δ_{str} is a sinusoidal function of 2φ . We also find that⁵⁴ μ_{str} , Δ_{Far} , and μ_{Far} are sinusoidal functions of 2φ . Remarkably, for a set of

nanoparticles positioned on a helix $\Delta_2 \neq 0$ and $\mu_2 \neq 0$, see Eq. (2).

For an arbitrary set of N nanoparticles, we cannot provide exact analytical expressions for $\Delta(\varphi)$ and $\mu(\varphi)$, or numerically explore the whole parameter space. In other words, the (narrow) windows of parameters where $\Delta(\varphi)$ and $\mu(\varphi)$ are nonsinusoidal functions of 2φ are not known. However, encouraged by the success of Eq. (2) in describing the optical behavior of a bulk medium²⁵ and a dimer, we propose to measure the well-defined quantities

$$\begin{aligned} \overline{\Delta_2} &= \int_0^\pi \Delta_{\text{str}}(\varphi) \frac{d\varphi}{\pi}, & \overline{\mu_2} &= \int_0^\pi \mu_{\text{str}}(\varphi) \frac{d\varphi}{\pi}, \\ \overline{\Delta_4} &= \int_0^\pi B \Delta_{\text{Far}}(\varphi) \frac{d\varphi}{\pi}, & \overline{\mu_4} &= \int_0^\pi B \mu_{\text{Far}}(\varphi) \frac{d\varphi}{\pi}, \end{aligned} \quad (27)$$

to study correlation between the geometry and the magneto-optical response of a set of nanoparticles. Figure 7(c) shows $\overline{\Delta_2}$, $\overline{\mu_2}$, $\overline{\Delta_4}$, and $\overline{\mu_4}$ of our helical structure as a function of the wavelength $2\pi c/\omega$. $\overline{\Delta_2}$ gains its minimum -0.023° and its maximum 0.011° at wavelengths of 384 and 397 nm, respectively. $\overline{\mu_2}$ reaches its maximum 0.026° at wavelength 388 nm. Note that near the same wavelengths, the circular dichroism spectrum is extremum. Similar to $\overline{\Delta_2}$, $\overline{\Delta_4}$ has a deep minimum -0.023° at 384 nm; however, $\overline{\Delta_2}$ and $\overline{\Delta_4}$ are distinct. Notably, $\overline{\Delta_2}$, $\overline{\mu_2}$, $\overline{\Delta_4}$, and $\overline{\mu_4}$ have the same order of magnitude.

V. RANDOM GAS OF NANOPARTICLES

We now consider a random arrangement of N identical nanoparticles of radius a [see Fig. 1(d)]. We rely on Na^3/R_g^3 as the volume fraction of the cluster. The radius of gyration R_g which characterizes the size of the system is defined as $R_g^2 = \frac{1}{N} \sum_{i=1}^N |\mathbf{r}_i - \mathbf{r}_{\text{cm}}|^2$. Here \mathbf{r}_{cm} is the position vector of the center of mass.

Intuitively, a random gas of nanoparticles is anisotropic and chiral to some extent. One can quantify chirality of a set of points through the Hausdorff chirality measure.⁵⁵ To characterize the anisotropy of the cluster, one can calculate the moment of inertia tensor $I_{\alpha\beta} = \sum_{i=1}^N \delta_{\alpha\beta} \mathbf{r}_i \cdot \mathbf{r}_i - (\mathbf{r}_i)_\alpha (\mathbf{r}_i)_\beta$ and its three real eigenvalues $I_1 \leq I_2 \leq I_3$. Then an appropriate function of the principal moments of inertia, e.g., $I_1/(I_1 + I_2 + I_3)$, serves as a measure of anisotropy.

We study a set of 1000 silver nanoparticles of radius $a = 10$ nm, which are distributed in an ellipsoid with semiaxes lengths of 10, 30, and 58 μm . Deliberately, we did not allow the particles to be nearer than $3a$. The volume fraction of the sample is about 0.05. We further assume that $\mathbf{k} \parallel \hat{z}$, $\mathbf{B} \parallel \hat{z}$ and $\varepsilon_m = 1.7$. Our cluster exhibits circular dichroism [see Fig. 8(a)]. The spectrum has three maxima and three minima, whose position and magnitude are almost independent of B . We observe that⁵⁴ Δ_{str} , μ_{str} , Δ_{Far} , and μ_{Far} are sinusoidal functions of 2φ [see Fig. 8(b)]. Remarkably, for a random gas of nanoparticles, all $\overline{\Delta_2}$, $\overline{\mu_2}$, $\overline{\Delta_4}$, and $\overline{\mu_4}$ are nonzero and have the same order of magnitude [see Fig. 8(c)]. As expected, the wavelengths at which $\sigma_+ - \sigma_-$, $\overline{\Delta_2}$, $\overline{\mu_2}$, $\overline{\Delta_4}$, and $\overline{\mu_4}$ are extremum, are quite close.

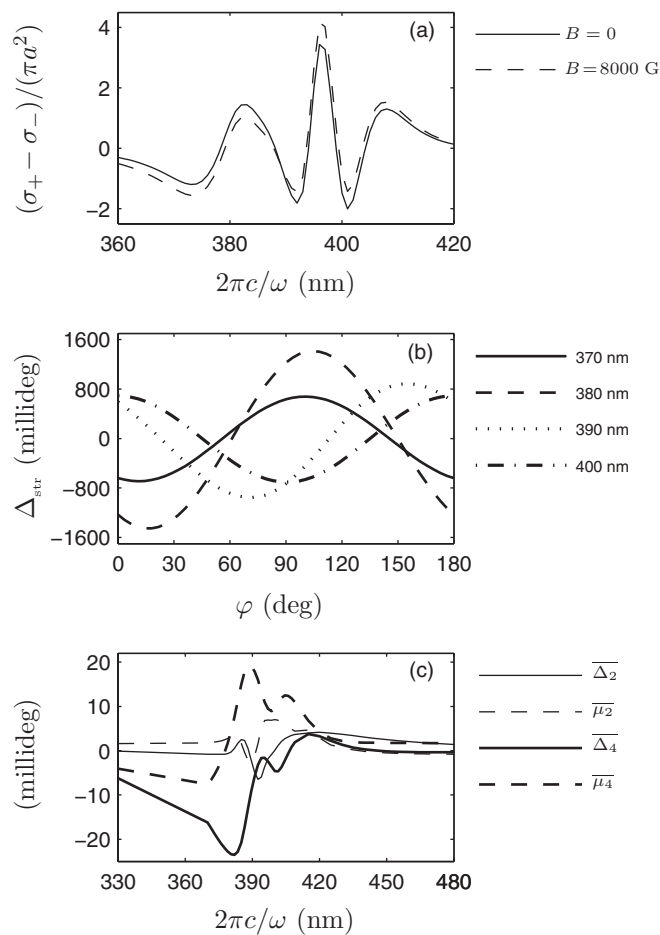


FIG. 8. Magneto-optical response of 1000 silver nanoparticles distributed in an ellipsoid. $a = 10$ nm and $\epsilon_m = 1.7$. (a) $(\sigma_+ - \sigma_-)/(\pi a^2)$ as a function of $2\pi c/\omega$. (b) Δ_{str} as a function of φ , for various wavelengths $2\pi c/\omega$. (c) $\overline{\Delta}_2$, $\overline{\mu}_2$, $\overline{\Delta}_4$, and $\overline{\mu}_4$ as a function of $2\pi c/\omega$. Here $\mathbf{k} \parallel \hat{z}$ and $\mathbf{B} = 8000 \text{ G}\hat{z}$.

VI. DISCUSSION

On propagation through a bulk medium, a linearly polarized electromagnetic wave becomes elliptically polarized. The polarization azimuth rotation and ellipticity angle variation are due to optical anisotropy and optical activity of the bulk medium. The constitutive equation $4\pi \mathbf{P}_\alpha = (\epsilon_{\alpha\beta} - \delta_{\alpha\beta})\mathbf{E}_\beta + \Gamma_{\alpha\beta\gamma} \nabla_\gamma \mathbf{E}_\beta$ gives the polarization of the bulk medium \mathbf{P} in terms of the electric field \mathbf{E} . Here $\epsilon_{\alpha\beta}$ are components of the dielectric tensor describing anisotropy and $\Gamma_{\alpha\beta\gamma}$ are components of the nonlocality tensor describing optical activity.²⁵ In isotropic optically active media, $\epsilon_{\alpha\beta} = n^2 \delta_{\alpha\beta}$ and $\Gamma_{\alpha\beta\gamma} = \Gamma e_{\alpha\beta\gamma}$, where n is the complex refractive index and $e_{\alpha\beta\gamma}$ is the Levi-Civita symbol. If a left (right) circularly polarized light is incident on the isotropic optically active medium, it will propagate as a left (right) circularly polarized light. The eigenpolarizations of an anisotropic medium with no optical activity ($\Gamma_{\alpha\beta\gamma} = 0$) are two linearly polarized waves. In general, one can measure the polarization azimuth rotation Δ and ellipticity angle variation μ as a function of the azimuth φ of an initially polarized wave, to separate the optical anisotropy and the optical activity of bulk medium.²⁵

A nanoparticle assembly is anisotropic and chiral to some extent. We showed that, to a good approximation, the structural polarization azimuth rotation and the structural ellipticity angle variation of a cluster are sinusoidal functions of 2φ [see Eq. (2)]. Studying the dimer, the helical arrangement, and the random gas of nanoparticles, we inferred that the amplitude Δ_1 and the offset Δ_2 inform us about the anisotropy and chirality of the cluster, respectively. Further studies are needed to quantify anisotropy and chirality of the nanoparticle assembly and quantify their link to Δ_1 and Δ_2 . Δ_1 and Δ_2 of a random gas of 1000 silver nanoparticles are of the order of 1° and 0.01° respectively, [see Figs. 8(b) and 8(c)]. Experimental measurement of these angles is not difficult.

In the presence of an external magnetic field 10 000 G, bulk gold exhibits very weak MO response. Indeed, at wavelength 700 nm, $\epsilon_{xy} = 10^{-4} + i10^{-3}$ for gold, whereas $\epsilon_{xy} = 0.8 + i0.16$ for cobalt.²³ However, the off-diagonal terms of the polarizability tensor of an isolated metal nanoparticle becomes considerably large near the surface plasmon frequency²³ [see Eqs. (7) and (8)]. Hui and Stroud studied Faraday rotation of a dilute suspension of particles in a host. Relying on the Maxwell-Garnett approximation, they also found that the Faraday effect becomes large near the surface plasmon frequency.⁵⁶ The effective medium or “mean-field” approximations do not take into account the interaction between particles. Thus we relied on coupled-dipole equations. Considering interacting nanoparticles, we found that Faraday rotation and Faraday ellipticity are also sinusoidal functions of 2φ . Remarkably, Faraday rotation and Faraday ellipticity of both helical arrangement and random gas of silver nanoparticles are of the order 0.01° [see Figs. 7(c) and 8(c)].

Recently Kuzyk *et al.*³² used DNA origami to create left- and right-handed nanohelices of diameter 34 nm and helical pitch 57 nm by nine gold nanoparticles of radius 5 nm. They even achieved spectral tuning of CD by metal composition. By depositing several nanometers of silver on gold nanoparticles, a blueshift of the CD peak was observed. In their pioneering work, Fan and Govorov³⁰ assumed that helical arrangement of nanoparticles are in a solution and have random orientations. Thus they performed averaging over the various directions of light wave vector \mathbf{k} to compute the CD spectrum. We envisage an ensemble of aligned helical structures; thus we emphasized the dependence of the CD spectrum on the direction of \mathbf{k} [see Fig. 7(a)]. First, we remember that various techniques are developed to align nanorods,⁵⁷ e.g., gold nanorods are incorporated within poly(vinyl alcohol) thin films and subsequently aligned by heating and stretching the film.⁵⁸ Nanohelices maybe aligned by the same procedures. Second, we believe that the light pressure can be invoked to generate and align helical arrangement of nanoparticles. Nahal *et al.*⁵⁹ reported generation of spontaneous periodic structures in AgCl-Ag films. The AgCl layer acts as a waveguide. The incident light scattered by the Ag nanoparticles excites waveguide modes which interfere with the incident beam. Silver nanoparticles then immigrate to the minima of the interference pattern. Electron microphotographs of samples irradiated by a circularly polarized light suggest the formation of helical arrangement of nanoparticles. This is further supported by the circular dichroism of the sample and recent atomic

force and scanning electron microscopy (AFM and SEM) images.⁶⁰

We anticipated that the simplest cluster, a dimer, has interesting MO properties. Two-dimensional arrangements of dimers can be produced by electron-beam lithography.⁶¹ Molecular bridges can also be employed to form Au and Ag dimers, trimers, and tetramers.^{62,63}

Our work can be extended in many directions. MO response of trimers, tetramers, two-dimensional arrangements of particles, fractal clusters, and the influence of particle size dispersion^{64–67} are of immediate interest. We envisage the *optical control* of the MO response of a solution of molecularly bridged dimers. Some molecular bridges, for example, azobenzene derivatives, reversibly transform between *trans* and *cis* conformations upon light radiation. Thus the dimer length and its MO properties can be optically controlled.

ACKNOWLEDGMENT

We would like to thank A. Nahal from the University of Tehran for fruitful discussions.

APPENDIX: THE PARAMETERS J_1 – J_7

The parameters J_1 – J_7 , introduced in Eq. (23), can be written as

$$\begin{aligned}
 J_0 &= |\alpha_{xx} - \eta\alpha_{xx}^2|^2 + |\alpha_{xx} - (\eta + \xi)\alpha_{xx}^2|^2, \\
 J_1 &= \frac{2}{J_0} \text{Re}[(\alpha_{xx} - \eta\alpha_{xx}^2)(\alpha_{xx}^* - (\eta^* + \xi^*)\alpha_{xx}^{*2})], \\
 J_2 &= \frac{1}{J_0} [|\alpha_{xx} - \eta\alpha_{xx}^2|^2 - |\alpha_{xx} - (\eta + \xi)\alpha_{xx}^2|^2], \\
 J_3 &= \frac{2}{J_0} \text{Re}[(\alpha_{xx} - \eta\alpha_{xx}^2)\mathcal{F}^* + (\alpha_{xx}^* - (\eta^* + \xi^*)\alpha_{xx}^{*2})\mathcal{F}], \\
 J_4 &= \frac{2}{J_0} \text{Re}[(\alpha_{xx} - \eta\alpha_{xx}^2)\mathcal{F}^* - (\alpha_{xx}^* - (\eta^* + \xi^*)\alpha_{xx}^{*2})\mathcal{F}], \\
 J_5 &= \frac{2}{J_0} \text{Im}[(\alpha_{xx} - \eta\alpha_{xx}^2)(\alpha_{xx}^* - (\eta^* + \xi^*)\alpha_{xx}^{*2})], \\
 J_6 &= \frac{-2}{J_0} \text{Im}[(\alpha_{xx} - \eta\alpha_{xx}^2)\mathcal{F}^* + (\alpha_{xx}^* - (\eta^* + \xi^*)\alpha_{xx}^{*2})\mathcal{F}], \\
 J_7 &= \frac{-2}{J_0} \text{Im}[(\alpha_{xx} - \eta\alpha_{xx}^2)\mathcal{F}^* - (\alpha_{xx}^* - (\eta^* + \xi^*)\alpha_{xx}^{*2})\mathcal{F}].
 \end{aligned}
 \tag{A1}$$

*mirfaez_miri@ut.ac.ir

¹A. Zvezdin and V. Kotov, *Modern Magneto-optics and Magneto-optical Materials* (IOP, Bristol, 1997).

²Š. Višňovský, *Optics in Magnetic Multilayers and Nanostructures* (Taylor and Francis, Boca Raton, FL, 2006).

³R. F. Ziolo, E. P. Giannelis, B. A. Weinstein, M. P. O'Horo, B. N. Ganguly, V. Mehrotra, M. W. Russell, and D. R. Huffman, *Science* **257**, 219 (1992).

⁴B. X. Gu, *Appl. Phys. Lett.* **82**, 3707 (2003).

⁵D. A. Smith, Y. A. Barnakov, B. L. Scott, S. A. White, and K. L. Stokes, *J. Appl. Phys.* **97**, 10M504 (2005).

⁶F. Bentivegna, M. Nyvlt, J. Ferré, J. P. Jamet, A. Brun, Š. Višňovský, and R. Urban, *J. Appl. Phys.* **85**, 2270 (1999).

⁷C. Clavero, A. Cebollada, G. Armelles, Y. Huttel, J. Arbiol, F. Peiró, and A. Cornet, *Phys. Rev. B* **72**, 024441 (2005).

⁸C. Clavero, G. Armelles, J. Mangueritat, J. Gonzalo, M. García del Muro, A. Labarta, and X. Batlle, *Appl. Phys. Lett.* **90**, 182506 (2007).

⁹K. S. Buchanan, A. Krichevsky, M. R. Freeman, and A. Meldrum, *Phys. Rev. B* **70**, 174436 (2004).

¹⁰V. I. Belotelov, I. A. Akimov, M. Pohl, V. A. Kotov, S. Kasture, A. S. Vengurlekar, A. V. Gopal, D. R. Yakovlev, A. K. Zvezdin, and M. Bayer, *Nat. Nanotechnol.* **6**, 370 (2011).

¹¹A. B. Khanikaev, A. V. Baryshev, A. A. Fedyanin, A. B. Granovsky, and M. Inoue, *Opt. Express* **15**, 6612 (2007).

¹²V. I. Belotelov, L. L. Doskolovich, and A. K. Zvezdin, *Phys. Rev. Lett.* **98**, 077401 (2007).

¹³Y. M. Strel'niker and D. J. Bergman, *Phys. Rev. B* **77**, 205113 (2008).

¹⁴Y. M. Strel'niker and D. J. Bergman, *Phys. Rev. B* **59**, R12763 (1999).

¹⁵D. J. Bergman and Y. M. Strel'niker, *Phys. Rev. Lett.* **80**, 857 (1998).

¹⁶T. Katayama, Y. Suzuki, H. Awano, Y. Nishihara, and N. Koshizuka, *Phys. Rev. Lett.* **60**, 1426 (1988).

¹⁷E. Ferreira-Vila, J. B. González-Díaz, R. Fermento, M. U. González, A. García-Martín, J. M. García-Martín, A. Cebollada, G. Armelles, D. Meneses-Rodríguez, and E. M. Sandoval, *Phys. Rev. B* **80**, 125132 (2009).

¹⁸E. Ferreira-Vila, M. Iglesias, E. Paz, F. J. Palomares, F. Cebollada, J. M. González, G. Armelles, J. M. García-Martín, and A. Cebollada, *Phys. Rev. B* **83**, 205120 (2011).

¹⁹P. K. Jain, Y. H. Xiao, R. Walsworth, and A. E. Cohen, *Nano Lett.* **9**, 1644 (2009).

²⁰R. K. Dani, H. Wang, S. H. Bossmann, G. Wysin, and V. Chikan, *J. Chem. Phys.* **135**, 224502 (2011).

²¹Y. Li, Q. Zhang, A. V. Nurmikko, and S. Sun, *Nano Lett.* **5**, 1689 (2005).

²²D. A. Smith and K. L. Stokes, *Opt. Express* **14**, 5746 (2006).

²³B. Sepúlveda, J. B. González-Díaz, A. García-Martín, L. M. Lechuga, and G. Armelles, *Phys. Rev. Lett.* **104**, 147401 (2010).

²⁴S. K. Ghosh and T. Pal, *Chem. Rev.* **107**, 4797 (2007).

²⁵Yu. P. Svirko and N. I. Zheludev, *Polarization of Light in Nonlinear Optics* (Wiley, Chichester, 1998).

²⁶C. A. Emeis, L. J. Oosterhoff, and Gonda de Vries, *Proc. R. Soc. London A* **297**, 54 (1967).

²⁷V. P. Drachev, W. D. Bragg, V. A. Podolskiy, V. P. Safonov, W. Kim, Z. C. Ying, R. L. Armstrong, and V. M. Shalaev, *J. Opt. Soc. Am. B* **18**, 1896 (2001).

²⁸V. Yannopoulos, *Opt. Lett.* **34**, 632 (2009).

²⁹E. Plum, V. A. Fedotov, and N. I. Zheludev, *J. Opt. A: Pure Appl. Opt.* **11**, 074009 (2009).

³⁰Z. Fan and A. O. Govorov, *Nano Lett.* **10**, 2580 (2010).

³¹Z. Fan and A. O. Govorov, *J. Phys. Chem. C* **115**, 13254 (2011).

³²A. Kuzyk, R. Schreiber, Z. Fan, G. Pardatscher, E. Roller, A. Högele, F. C. Simmel, A. O. Govorov, and T. Liedl, *Nature (London)* **483**, 311 (2012).

³³N. B. Baranova and B. Ya Zeldovich, *Mol. Phys.* **38**, 1085 (1979).

- ³⁴G. H. Wagnière and A. Meier, *Chem. Phys. Lett.* **93**, 78 (1982).
- ³⁵L. D. Barron and J. Vrbancich, *Mol. Phys.* **51**, 715 (1984).
- ³⁶G. L. J. A. Rikken and E. Raupach, *Nature (London)* **390**, 493 (1997).
- ³⁷L. D. Barron, *Molecular Light Scattering and Optical Activity* (Cambridge University Press, Cambridge, UK, 2004).
- ³⁸D. L. Portigal and E. Burstein, *J. Phys. Chem. Solids* **32**, 603 (1971).
- ³⁹A. H. Sihvola, *Opt. Lett.* **19**, 430 (1994).
- ⁴⁰A. Vial and T. Laroche, *Appl. Phys. B* **93**, 139 (2008).
- ⁴¹P. B. Johnson and R. W. Christy, *Phys. Rev. B* **6**, 4370 (1972).
- ⁴²H. Hövel, S. Fritz, A. Hilger, U. Kreibig, and M. Vollmer, *Phys. Rev. B* **48**, 18178 (1993).
- ⁴³E. A. Coronado and G. C. Schatz, *J. Chem. Phys.* **119**, 3926 (2003).
- ⁴⁴U. Kreibig and L. Genzel, *Surf. Sci.* **156**, 678 (1985).
- ⁴⁵U. Kreibig and M. Vollmer, *Optical Properties of Metal Clusters* (Springer, Berlin, 1995).
- ⁴⁶J. D. Jackson, *Classical Electrodynamics* (Wiley, New York, 1975).
- ⁴⁷*Optics of Nanostructured Materials*, edited by V. A. Markel and T. F. George (Wiley, New York, 2001).
- ⁴⁸V. M. Shalaev, *Nonlinear Optics of Random Media: Fractal Composites and Metal-Dielectric Films* (Springer-Verlag, Berlin, 2000).
- ⁴⁹V. A. Markel, V. M. Shalaev, E. B. Stechel, W. Kim, and R. L. Armstrong, *Phys. Rev. B* **53**, 2425 (1996).
- ⁵⁰S. V. Perminov, S. G. Rautian, and V. P. Safonov, *J. Exp. Theor. Phys.* **98**, 691 (2004).
- ⁵¹V. A. Kosobukin and B. B. Krichevstov, *Phys. Solid State* **52**, 813 (2010).
- ⁵²C. F. Bohren and D. R. Huffman, *Absorption and Scattering of Light by Small Particles* (Wiley, New York, 1983).
- ⁵³E. Collett, *Polarized Light: Fundamentals and Applications* (Marcel Dekker, New York, 1993).
- ⁵⁴For the sake of brevity, data are not shown here.
- ⁵⁵A. B. Buda and K. Mislow, *J. Am. Chem. Soc.* **114**, 6006 (1992).
- ⁵⁶P. M. Hui and D. Stroud, *Appl. Phys. Lett.* **50**, 950 (1987).
- ⁵⁷L. M. Liz-Marzán, *Langmuir* **22**, 32 (2006).
- ⁵⁸J. Pérez-Juste, B. Rodríguez-González, P. Mulvaney, and L. M. Liz-Marzán, *Adv. Funct. Mater.* **15**, 1065 (2005).
- ⁵⁹A. Nahal, V. K. Miloslavsky, and L. A. Ageev, *Opt. Commun.* **154**, 234 (1998).
- ⁶⁰A. Nahal and R. Talebi (unpublished).
- ⁶¹W. Rechberger, A. Hohenau, A. Leitner, J. R. Krenn, B. Lamprecht, and F. R. Aussenegg, *Opt. Comm.* **220**, 137 (2003).
- ⁶²L. C. Brousseau, J. P. Novak, S. M. Marinakos, and D. L. Feldheim, *Adv. Mater.* **11**, 447 (1999).
- ⁶³J. P. Novak and D. L. Feldheim, *J. Am. Chem. Soc.* **122**, 3979 (2000).
- ⁶⁴Z. Naeimi and M. F. Miri, *Phys. Rev. B* **80**, 224202 (2009).
- ⁶⁵Z. Naeimi and M. F. Miri, *J. Phys. Chem. C* **115**, 15251 (2011).
- ⁶⁶A. E. Ershov, I. L. Isaev, P. N. Semina, V. A. Markel, and S. V. Karpov, *Phys. Rev. B* **85**, 045421 (2012).
- ⁶⁷J. M. Zook, V. Rastogi, R. I. MacCusprie, A. M. Keene, and J. Fagan, *ACS Nano* **5**, 8070 (2011).